PHOTO-TRANSFERRED THERMOLUMINESCENCE CHARACTERISTICS OF BETA-IRRADIATED MgO NANOPOWDERS

A MASTER'S THESIS

in

Chemical Engineering and Applied Chemistry

Atilim University

by

ABEER MAMI

APRIL 2018

PHOTO-TRANSFERRED THERMOLUMINESCENCE CHARACTERISTICS OF BETA-IRRADIATED MgO NANOPOWDERS

A THESIS SUBMITTED TO

THE GRADUATE SCHOOL OF NATURAL AND APPLIED SCIENCES

OF

ATILIM UNIVERSITY

BY

ABEER MAMI

IN PARTIAL FULFILLMENT OF THE REQUIREMENTS FOR THE DEGREE OF MASTER OF SCIENCE

IN

APPLIED CHEMISTRY

AT CHEMICAL ENGINEERING AND APPLIED CHEMISTRY DEPARTMENT

APRIL 2018

Approval of the Graduate School of Natural and Applied Sciences, Atılım University.

_____

Prof. Dr. Ali Kara

Director

I certify that this thesis satisfies all the requirements as a thesis for the degree of Master of Science.

_____

Prof. Dr. Atilla Cihaner

Head of Department

This is to certify that we have read the thesis "Photo-Transferred Thermoluminescence Characteristics of Beta-Irradiated MgO Nanopowders" submitted by "Abber Mami" and that in our opinion it is fully adequate, in scope and quality, as a thesis for the degree of Master of Science.

_____

Assoc. Prof. Dr. Mehmet Işık

Supervisor

Examining Committee Members

Prof. Dr. Nizami Hasanli _____

Prof. Dr. Atilla Cihaner _____

Assoc. Prof. Dr. Belgin İşgör _____

Assoc. Prof. Dr. Seha Tirkeş _____

Assoc. Prof. Dr. Mehmet Işık _____

Date: 19.04.2018

I declare and guarantee that all data, knowledge and information in this document has been obtained, processed and presented in accordance with academic rules and ethical conduct. Based on these rules and conduct, I have fully cited and referenced all material and results that are not original to this work.

Name, Last name: Abeer, MAMI

Signature:

ABSTRACT

PHOTO-TRANSFERRED THERMOLUMINESCENCE CHARACTERISTICS OF BETA-IRRADIATED MgO NANOPOWDERS

Mami, Abeer

M.S., Department of Chemical Engineering and Applied Chemistry

Supervisor: Assoc. Prof. Dr. Mehmet Işık

April 2018, 39 pages

Shallow trapping centers in MgO nanopowders were characterized using photo-transferred thermoluminescence measurements. Experiments were carried out in low temperature range of 10-300 K with constant heating rate. Shallow traps were filled with charge carriers firstly by irradiating the sample at room temperature using S90/Y90 source and then illuminating at 10 K using blue LED. Thermoluminescence glow curve exhibited one peak around 150 K. Curve fitting analyses showed that this peak is composed by individual peaks with maximum temperatures of 149.0 and 155.3 K. The activation energies of corresponding trapping centers were revealed as 0.70 and 0.91 eV. The dominant mechanism for TL process was found as second order kinetics which represent that fast retrapping is effective transitions taking place within the band gap. Analyses were also done using initial rise and peak shape methods. All results were in good agreement with each other.

Structural characterization of MgO nanopowders were investigated using x-ray diffraction, scanning electron microscopy and Fourier transform infrared spectroscopy measurements. Analyses of experimental observations indicated that MgO nanopowders show good crystallinity with particle size around 20-30 nm.

Keywords: Thermoluminescence, MgO, Defects

ÖZ

BETA-IŞINLANMIŞ MgO NANOTOZLARIN FOTO-TRANSFER TERMOLÜMİNESANS KARAKTERİSTİKLERİ

Mami, Abeer

Yüksek Lisans, Kimya Mühendisliği ve Uygulamalı Kimya Bölümü

Tez Yöneticisi: Doç. Dr. Mehmet Işık

Nisan 2018, 39 sayfa

MgO nanotozlarındaki sığ tuzak merkezleri foto-transfer termolüminesans ölçümleri kullanılarak karakterize edildi. Deneyler sabit ısıtma hızı ile 10-300 K düşük sıcaklık aralığında gerçekleştirildi. Sığ tuzak merkezleri ilk olarak oda sıcaklığında S90/Y90 kaynağı ile ışıma yaptırarak ve daha sonra 10 K sıcaklığında mavi LED kullanılarak ışıklandırarak yük taşıyıcıları ile dolduruldu. Termolüminesans eğrisi 150 K civarında bir pik gösterdi. Eğri fit analizleri bu pikin maksimum sıcaklıkları 149.0 ve 155.3 K olan iki birbirinden ayrı pikten oluştuğunu gösterdi. Piklere karşılık gelen tuzak merkezlerinin aktivasyon enerjileri 0.70 ve 0.91 eV olarak ortaya çıkarıldı. TL süreçlerindeki baskın mekanizma, hızlı geri tuzaklanmanın bant boşluğu içerisinde gerçekleşen geçişlerde etkili olduğunu ifade eden ikinci dereceden mertebe olarak bulundu. Analizler ayrıca ilk yükselme ve pik şekli metotları kullanılarak yapıldı. Tüm sonuçlar birbirleri ile uyumluluk gösterdi.

MgO nanotozların yapısal karakterizasyonu x-ışını kırınımı, tarayıcı elektron mikroskobu ve Fourier dönüşümlü kızılötesi spektroskobi ölçümleri ile incelendi. Deneysel gözlemlerin analizleri MgO nanotozların 20-30 nm civarında parçacık boyutuna sahip iyi kristallik özelliği gösterdiğini işaret etti.

Anahtar Kelimeler: Termolüminesans, MgO, Kusurlar

To My Family

ACKNOWLEDGMENTS

I offer my sincere thanks and gratitude and all respect and appreciation to who enlighten the science of my way to my supervisor Assoc. Prof. Dr. Mehmet Işık. To the warm embrace and the affectionate chest and to who call were accompanied to my beloved mother. To the high mountain and the strong bridge and to the spring flowing with tender without waiting for the return to who taught me that life is a work and a gift to my father. To who supported me in my way and was helping me in my career and was scientific in the moments of my studies my dear husband. To the light of my eyes, my beloved to my children. I required from my God Almighty to make my message a good beginning and a good nucleus on the path of science and light.

TABLE OF CONTENTS

ABSTRACT vi

OZ v

DEDICATION..... vi

ACKNOWLEDGMENTS vii

TABLE OF CONTENTS viii

LIST OF TABLES x

LIST OF FIGURES xi

CHAPTER

1. INTRODUCTION 1
2. THEORETICAL APPROACH ……..... 4

2.1 Introduction……..... 4

2.2 Band Structure of Solids.....4

2.3 Defects……6

2.3.1 Point defects.....7

2.3.2 Line defects.....7

2.3.3 Planar defects.....8

2.3.4 Volume/Bulk defects.....8

2.4 Doping…….....…9

2.5 Theoretical Approach to Experimental Methods……..…..9

2.5.1 X-ray diffraction.....9

2.5.2 Fourier Transform Infrared Measurements.....10

2.5.3 Thermoluminescence.....11

2.5.3.1 Electronic Transitions in TL Process…….....11

2.5.3.2 Theoretical Approach…….....13

2.5.3.3 Curve Fitting Method…….....14

2.5.3.4 Initial Rise Method…….....15

2.5.3.5 Peak Shape Method…….....15

3. EXPERIMENTAL DETAILS.....17

3.1 X-ray Diffraction …….....17

3.2 Scanning Electron Microscopy…….....17

3.3 Fourier Transform Infrared Spectroscopy.....19

3.4 Thermoluminescence Measurements….....19

4. RESULTS AND DISCUSSION.....21

4.1 Results of X-ray diffraction measurements.....21

4.2 Results of Scanning Electron Microscopy Measurements.....24

4.2 Results of FTIR Measurements.....26

4.2 Results of Thermoluminescence Measurements.....26

5. CONCLUSIONS 34

REFERENCES 36

LIST OF TABLES

4.1 X-ray powder diffraction data for MgO nanoparticles.....22

4.2 The activation energy (E_t) of traps for two TL peaks of MgO nanopowder.....31

LIST OF FIGURES

2.1 (a) Schematic presentation of the potential energy of an electron in a one-dimensional crystal structure. (b) Kronig-Penney model approximation….....5

2.2 Simple diagram of the reduced-zone representation.....5

2.3 Energy bands in solids……...6

2.4 Representation of various point defect types……..…7

2.5 (a) Edge dislocation; (b) Screw dislocation……8

2.6 X-ray diffraction from a crystal……..……10

2.7 Processes in FTIR experiments…….……...11

2.8 Possible electronic transitions in the TL..……....12

3.1 Rigaku miniflex diffractometer…….....18

3.2 Used scanning electron microscope……18

3.3 Nicolet 6700 FTIR spectrometer…….19

3.4 Simple diagram of low temperature thermoluminescence set-up……20

4.1 X-ray diffractogram of MgO nanoparticles…….22

4.2 Debye-Scherrer analyses according to Eq. 4.1……23

4.3 Williamson-Hall analyses of MgO nanopowders……24

4.4 SEM images of MgO nanoparticles…….25

4.5 Infrared transmittance spectrum of MgO nanopowders……..26

4.6 Simple diagram showing physical processes in TL experiments……...27

4.7 Simple diagram showing physical processes in PTTL experiments……....28

4.8 PTTL glow curve of MgO nanopowders…….…29

4.9 Experimental curve (stars) and fitted curves for slow retrapping (blue curve) and fast retrapping (red curve) cases……..30

4.10 Experimental TL curve (stars) and fitted curve (solid line). Dash-dotted curves represent the deconvoluted peaks……...…31

4.11 The plots for initial rise method analyses……...…32

4.12 Simple energy level diagram of MgO presenting transitions in PTTL……..33

CHAPTER 1

INTRODUCTION

Magnesium oxide (MgO) is an insulating material with gap energy of 7.8 eV (Tamboli et al., 2009). The electrical resistivity of the sample is on the order of 10^{20} Ω.cm at room temperature (Tardío et al., 2002). MgO presents rock-salt crystal structure (face centered cubic) at ambient temperature, and Mg ions occupy the octahedral position in the anionic compact packed structure.

MgO nanoparticles can be growth with desired size and morphology. There are many different growth morphologies of the MgO such as nanoparticles (Park et al., 2006), nanotubes, nano wires, nano belts (Yan et al., 2008), nanosheets (Selvam et al., 2011) and nanofibers (Shao et al., 2006). Thanks to these variety of growing morphologies, MgO takes attention in different technological areas such as photonic devices (Xu & Asher, 2004), confined catalysis (Shang et al., 2010), biotechnology (Zhao et al., 2011), electrochemical cells (Dong et al., 2011), drug delivery systems (Zhao et al., 2008) and luminescence (Devaraja et al., 2014). Different type of MgO samples have been used in different device applications due to their characteristic properties (Jalili & Majidi, 2008; Choudary et al., 2003; Stark & Klabunde, 1996; Huang et al., 2005). MgO is an effective sample used as a substrate for thin film growth and especially for superconducting thin film construction (Fletcher & Leach, 1995). MgO is chosen as one of the main materials studied because its effective atomic number is relatively low (Z_{eff} = 10.8).

Defects affecting many properties of the samples are the imperfections that damage the periodicity of the crystal structure. Moreover, these imperfections take an important role in the radiative emissions. Thermoluminescence (TL) is one of the

effective measurement techniques used to determine properties of defect levels for decades. In TL method, temperature versus TL intensity proportional to the emitted photons from the sample when the trapped charge carriers return to the valence band from defect centers. The curve of temperature-TL intensity called as TL glow curve is analyzed and properties of defect centers are obtained. Previously defetcs in the MgO samples were reported in many papers in the literature. TL characteristics of MgO crystals were searched in 170-500 K region to determine the properties of intrinsic defect centers (Kadri et al., 2005). UV irradiated MgO single crystal presented emission bands for F center at 540 nm, F^+ center at 380 nm, F_2 center at 350 nm and F_{cat} center at 290 nm. Photoluminescence, scintillation and thermoluminescence dosimeter properties of MgO ceramics doped with Mn^{2+} ion were reported by Kato et. al. (Kato et. al., 2016a). All samples doped with different concentration of Mn^{2+} present a PL emission around 730 nm. It was observed that PL intensity increases with increasing doping concentration. TL glow curves of X-ray irradiated samples exhibited one single peak around 140 ^oC. The dose dependence of TL intensity was reported as linear for Mn^{2+} doped MgO ceramics. One of the old studies on the TL properties of MgO was reported in 1978 (Sathyamoorthy & Luthra, 1978). TL glow curve of exhibited peaks around 365, 435, 510, 545 and 650 K.

The dosimetric and luminescence properties of MgO co-doped with Li, Ce and Sm were investigated by thermoluminescence and optically stimulated luminescence techniques (Oliveira et al., 2016). TL glow curves of all studied samples were considered and a possible model for TL mechanism was proposed by authors. The interesting observation in the TL glow curves is reported as that Sm^{3+} doped MgO presents a new TL peak around 180 ^oC. When Ce^{3+} was introduced to this sample it was observed that TL signal is enhanced and Ce^{3+} acts as luminescent center.

MgO ceramics were previously searched as TL dosimetric detector (Kato et. al., 2016b). TL curves recorded for all studied ceramics presented peaks ~85 and 140 ^oC. As the doping concentration was increased, it was observed that TL intensity decreases and TL peak maximum temperature shifts to lower temperature. The activation energies of the 0.001%, 0.01% and 0.1% Cr doped MgO ceramics were

found as 0.29, 0.21 and 0.15 eV, respectively. Frequency factors of the revealed trapping centers were also reported in this paper.

Thermoluminescence and optically stimulated luminescence properties of MgO doped with Nd and Li were investigated for 2D dosimetry (Oliveira et al., 2013a). Co-doped (Ni+Nd) effect on the TL response was also studied in this report. It was observed that Li co-doping with Nd increases the TL intensity. The TL glow curve of MgO:Nd,Li presents four peaks around 80 ^{o}C, 215 ^{o}C, 280 ^{o}C nd 350 ^{o}C.

Luminescence properties of MgO:Li,Gd was studied in the temperature range of 0-450 ^{o}C. TL glow curve of MgO:$Li_{3\%}Gd_{1\%}$ present an intense peak around 300 ^{o}C and weak peaks at lower temperatures (Oliveira et al., 2013b). It was reported in this paper that co-doping of Li and Gd significantly increases the TL intensity compared to MgO:$Li_{3\%}$.

In the present thesis MgO nanoparticles were investigated using phototransferred TL measurements in the 10-300 K region. The defect center parameters were reported as a result of analyses of recorded TL curves. The structural properties of the samples were also investigated.

CHAPTER 2

THEORETICAL APPROACH

2.1 Introduction

MgO is one of the most effective insulators used in different technological applications. Thanks to its attractive optical and electrical properties, characterization of MgO takes an important role for related scientific areas. In the present chapter, theoretical background of band structure of solids and used experimental methods throughout the thesis are given.

2.2 Band Structure of Solids

Atoms are regularly positioned in three dimensions in the crystalline materials. Thus, an electron inside the crystalline solid obeys the Schrödinger's wave equation for periodic potential and wavefunction of the electron is given as

$$\psi(r) = u(r)\exp(ikr), \tag{2.1}$$

where $u(r) = u(r + a)$ is the Bloch function, k is the wave vector and r is the position vector. The motion of the electron in the crystal structure is simplified by Kronig-Penney model in which electron is thought inside a one-dimensional array of square potential barriers as given in Fig. 2.1 (Kronig & Penney, 1930).

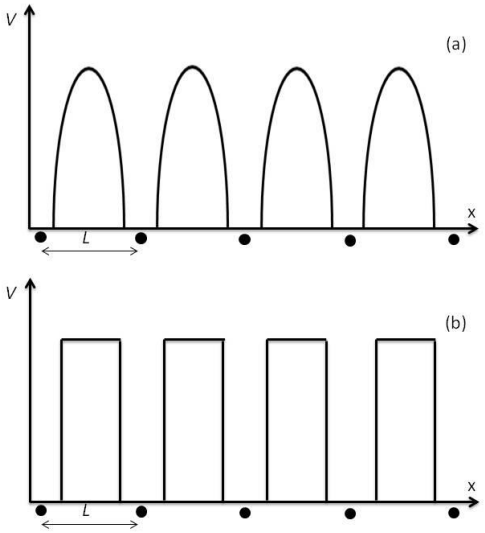

Figure 2.1. (a) Schematic presentation of the potential energy of an electron in a one-dimensional crystal structure. (b) Kronig-Penney model approximation (Yacobi 2003).

The results of the Scrödinger's wave equation points out two important consequences; Electrons can take only some allowed energy values and there exist discontinuities in energy at some wave vector values. The reduced-zone configuration and energy bands are presented in Fig. 2.2.

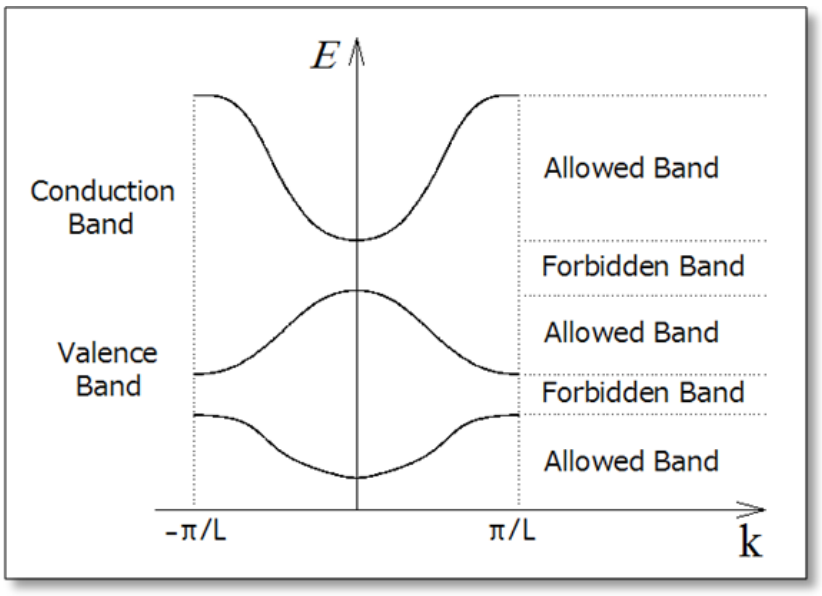

Figure 2.2. Simple diagram of the reduced-zone representation.

Band structure of solids presents two important bands called as valence and conduction bands. The highest energy band at which electrons can occupy at absolute zero temperature is called as valence band. The lowermost allowed energy band is named as conduction band. The energy value difference of valence and conduction bands is called as band gap energy. The helpful method to imagine the difference between a conductors, insulators and semiconductors are able to plot the obtainable energies used for electrons. The electrons in insulator occupy in the valence band due to wide gap between valence and conduction bands. There is sufficiently small gap between bands in the semiconductor and in the conductors, these bands overlap. Heat or additional excitement can bridge the gap. Figure 2.3 shows the simple configuration of energy bands in solids.

.

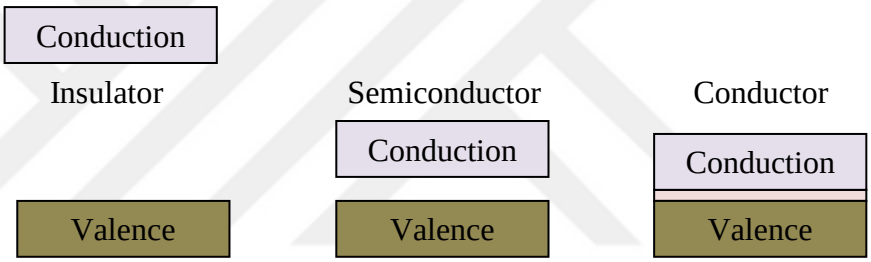

Figure 2.3 Energy Bands in Solids

2.3 Defects

Although the atoms are placed periodically in the crystalline solids, there can exist irregularities in the materials called as imperfection or defects. The structural, optical and electrical properties of the materials are affected due to the existence of different type of defects. According to the dimensions, defects are named as point, line, plane/surface and volume defects.

2.3.1 Point defects

These type of defects are dimensionless defects and emerge because of missing atom, extra atom or wrong location of an atom in crystal structure. Fig. 2.4 shows four types of point defects. *Self interstitial atoms* are extra atoms with the same type of bulk atoms in the crystal structure. They sit in irregular position in the lattice. *Substitutional impurity atoms* are different atoms from bulk ones and sit in the position of them. *Interstitial impurity atoms* are smaller atoms with the same type of bulk atoms and get position in the open areas between bulk atoms. *Vacancies* are the empty regions left by a missing atom.

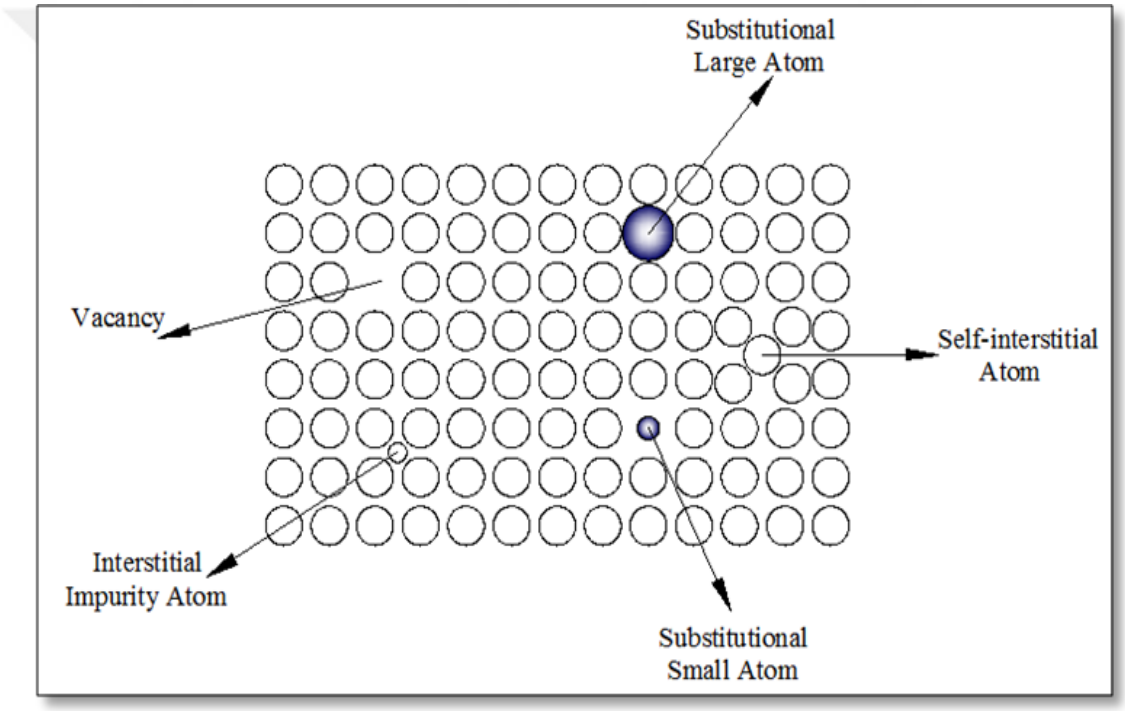

Figure 2.4. Representation of various point defect types.

2.3.2 Line defects

Line defects are called also as dislocations and exist due to the missing or wrong positions of the atom groups. There are two types of this one dimensional defects named as *edge* and *screw* dislocations shown in Fig. 2.5. Edge dislocations

come into existence when a plane is placed to or removed from the crystal structure. Screw dislocations are formed from a shear ripple stretching from side to side.

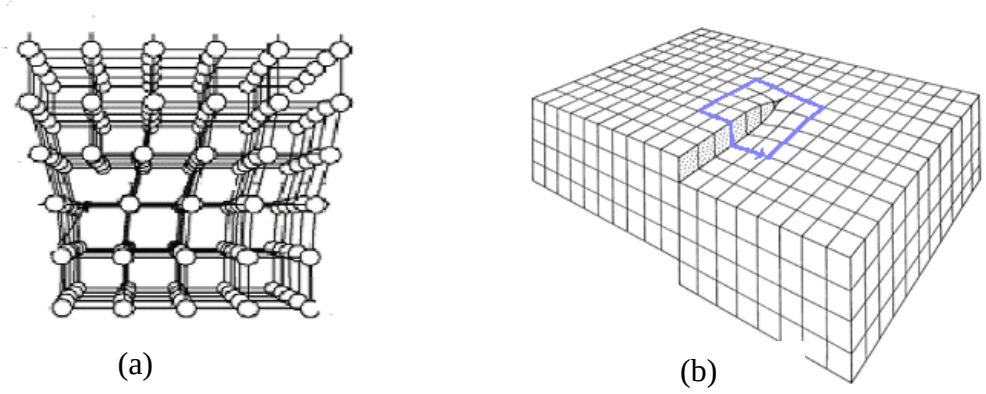

(a) (b)

Figure 2.5 (a) Edge dislocation; (b) Screw dislocation (Kittel 1967).

2.3.3 Planar defects

There are two main types of the two dimensional planar defects called as stacking faults and grain boundaries. Stacking fault exist due to a mistake in the sequence for a few atomic spacing. For example, if crystal arrangement of XYXYXYXY changes to XYXYXYZXY due to addition of a different atom Z, stacking faults are formed. If the arrangement XYXYXYXY changes to XYZXYZXYZ for a short period and then changes to initial arrangement, twin boundaries are formed. Real solids can consist of many small crystallites or grains. Various grains are separated by areas named as grain boundaries. Crystals having grains are called as polycrystals.

2.3.4 Volume/Bulk defects

Three dimensional volume/bulk defects are larger than previously mentioned defects. Voids, one of the general type of volume defects, are small areas in which

large amount of atoms are missing. Another type of volume defects, precipitates exist when impurities can cluster together and form small regions of a various type.

2.4 Doping

Doping is called as the addition of specific impurity to a solid to change its optical or electrical properties in the desired way. The main purpose of adding different specific atom to the host material is to increase the number of free carriers in the crystal structure. Previously, it is said that the energy region between the valence and conduction bands are forbidden. That means there is no any energy level(s) to be occupied by electrons. However, this theoretical fact is only valid for perfect crystalline solids that have no defects and/or impurities. Defects and impurities create additional energy levels in the forbidden energy region of the crystal structure.

2.5 Theoretical Approach to Experimental Methods

2.5.1 X-ray diffraction

It is the main techniques used in the structural characterization of crystalline materials. The inter distance of the atoms in the crystal lattice is in the order of nanometer. X-rays have also wavelengths in the same order of magnitude with the inter planar spacing of crystal structure. The wavelengths of the x-rays are in the range of 0.01-10 nm. The characterization of structural properties of crystalline materials gets use of elastic Thomson scattering. The diffracted x-ray from the different atoms as a result of elastic scattering from interference patterns. The constructive interference pattern helps us about the distribution of atoms in the crystalline material.

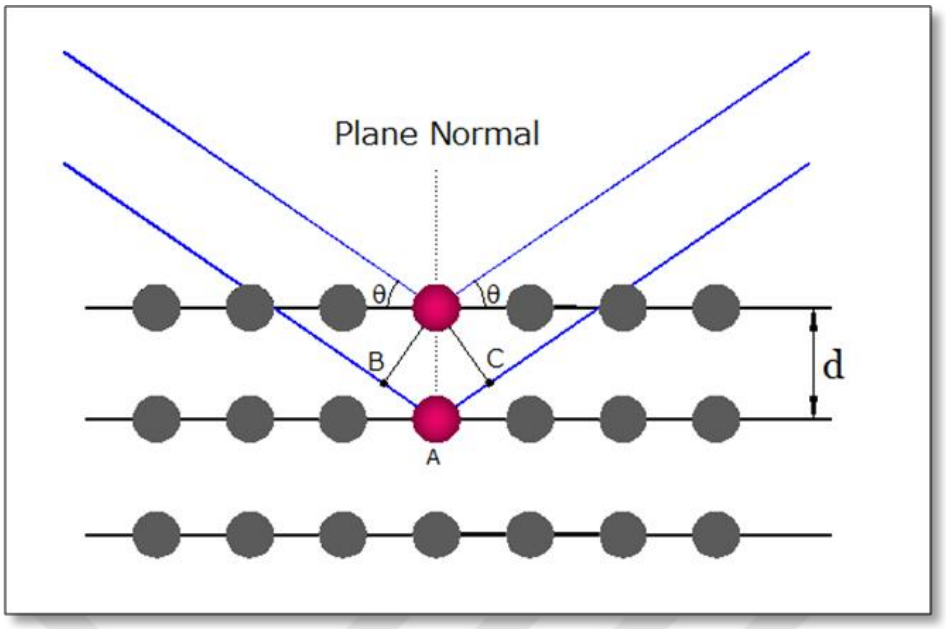

Figure 2.6 X-ray diffraction from a crystal.

Fig. 2.6 presents deflection of x-rays from a crystal lattice with a interplanar spacing of *d*. The path difference between the darker atoms in the figure is given as

$$|AB| + |AC| = 2d \sin\theta \tag{2.2}$$

If this difference is equal to integer multiple of λ, diffracted x-rays form a constructive interference. This is mathematically related as

$$2d_{hkl} \sin\theta = n\lambda \cdot \quad n = 0, 1, 2, 3.... \tag{2.3}$$

This relation is named as Bragg law and analysis of the observed XRD pattern is used to find the interplanar spacing, lattice constants, Miller indices and angles (Bragg, 1913).

2.5.2 Fourier Transform Infrared Measurements

FTIR spectroscopy experiments are performed to get infrared spectrum of the materials. In the experiments, infrared light passes through an interferometer and then through material (or vice versa). The distribution of infrared beam passing from

interferometer is changed by the help of a moving mirros. The interferogram shows light output depending on mirror position. The obtained data is changed to “light output as a function of wavenumber” using Fourier transform analyses. The spectrum of the sample is compared with a reference and resulting experimental data is obtained from this comparison. Figure 2.7 presents processes in the FTIR experiments.

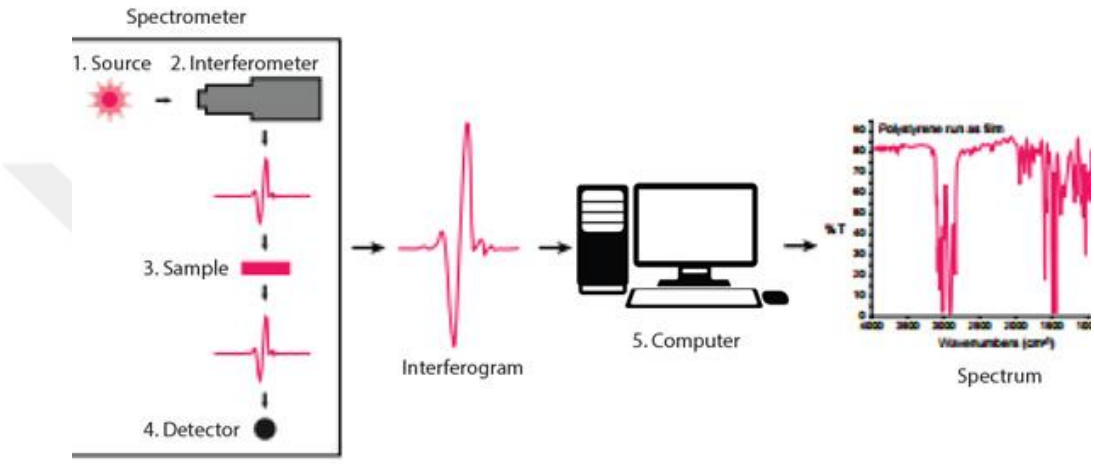

Figure 2.7. Processes in FTIR experiments

2.5.3 Thermoluminescence

Thermoluminescence is one of the basic experimental methods to get information about the trapping parameters of the materials. It is used for decades on the defect characterization of semiconductors and insulators. Theory of the thermoluminescence is mainly based on the transitions between localized and delocalized bands in the energy gap of the material. For that reason, it will be helpful to give knowledge about the possible electronic transitions occurring in the energy band gap.

2.5.3.1 Electronic Transitions in TL Process

In the perfect crystals, the energy gap between conduction and valence bands is forbidden. However, it is very difficult to have perfect crystal and every material contain some defect and/or impurities. These imperfections create an extra energy level(s) in this forbidden gap. TL is used to get information about this extra energy levels called as defect/trap center. In the TL process, there are some electronic transitions occurring between localized and delocalized energy levels. Fig. 2.8 presents a simple model of one trap level (T) and one recombination level (R). The possible transitions in the TL processes are given in detailed below.

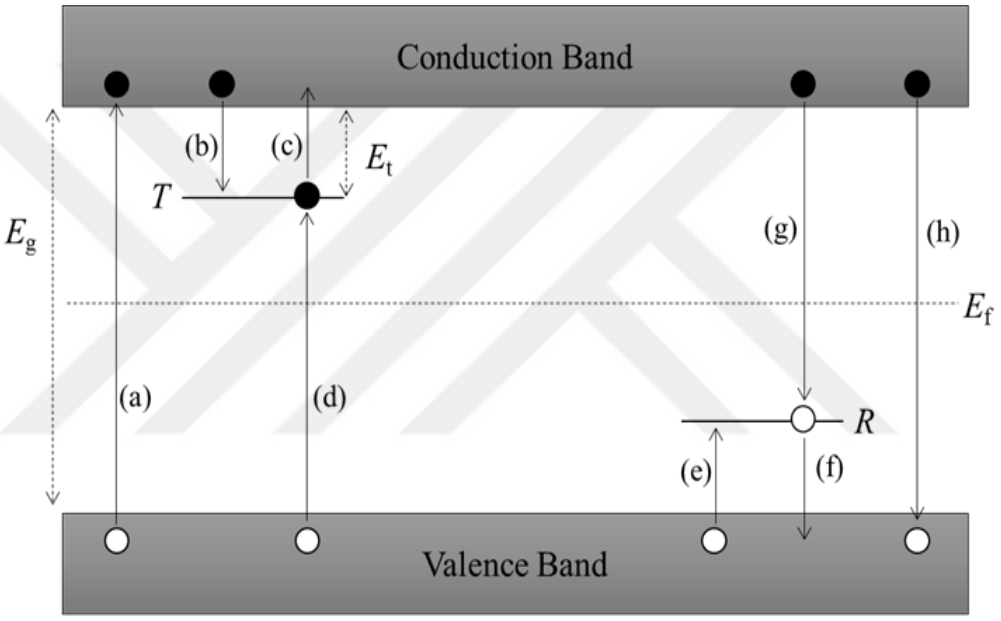

Figure 2.8. Possible electronic transitions in the TL. [McKeever 1985].

(I) Transition (a): When sample is radiated with a light source having energy bigger than gap energy, electrons are excited to conduction band from valence band. This results in free electrons and holes. Since this transition occurs between valence and conduction bands, it is named as band-to-band transition.

(II) Transitions (b) and (e): The excited electrons either make recombination with holes or trapped in the defect centers. This possibility also exist for free holes in VB band. Transitions (b) and (e) shows trapping of electrons and holes, respectively.

(III) Transition (h): Another possibility for free electrons is to make direct transition which is the recombination of free electrons and holes. This transition is shown in the figure by “h”.

(IV) Transitions (c) and (f): When trapped electrons and holes get energy to be excited from trap centers, they make transitions (c) and (f), respectively, shown in the figure. In the TL measurements, this energy is supplied by means of temperature.

(V) Transitions (g) and (d): These transitions are called as indirect transition occuring between opposite charge carriers though one localized and one delocalized band.

TL simple model: The sample at a low temperature is radiated by a suitable light source to excite the electrons occupying in the valence band to conduction band. Most of the excited electrons make direct recombination. However, some of the electrons are captured by defect centers. When the radiation is turned off, the trapped charge carriers remain in the related trap centers. In the TL process, the sample is heated in dark. The energy supplied by heat can give possibility to trapped carriers to escape from the trap centers. The electrons escaping from trap centers to conduction band return to valence band. When these electrons maket his transition, the energy difference between the energy levels are given as photon to outside. Temperature dependence of count of these photons are obtained as a result of thermoluminescence experiments. This dependency curve called as glow curve is analyzed to find the trapping parameters such activation energy, escape frequency, order of kinetics.

2.5.3.2 Theoretical Approach

Thermoluminescence intensity is theoretically defined for three different case; first order of kinetics (slow retrapping), second order of kinetics (fast retrapping) and general order of kinetics. As mentioned above, charge carriers are excited to delocalized bands when they get sufficient energy. If these charge carriers return back to trap levels and takes role in TL process more than one time, retrapping case occurs. This affect the shape of the TL glow curve and theoretical equations differ

for each of kinetics case. TL intensity is given for each case as (McKeever 1985, Chen & Kirsh 1981)

$$I_{TL} = n_0 \nu \exp\left\{ -\frac{E}{kT} - \int_{T_0}^{T} \frac{\nu}{\beta} \exp(-E/kT) dT \right\} . \quad (2.4)$$

$$I_{TL} = -\frac{dn}{dt} = \left(\frac{n_0^2}{N} \right) \nu \exp\left[-\frac{E}{kT} \right] \left[1 + \frac{n_0 \nu}{\beta N} \int_{T_0}^{T} \exp(-E/kT)\, dT \right]^{-2} \quad (2.5)$$

$$I_{TL} = n_0 \nu \exp\left(-\frac{E_t}{kT} \right) \left[1 + (b-1) \frac{\nu}{\beta} \int_{T_0}^{T} \exp(-E_t/kT) dT \right]^{-\frac{b}{b-1}} \quad (2.6)$$

Eqs. 2.4, 2.5 and 2.6 corresponds to slow retrapping, fast retrapping and mixed order of kinetics, respectively. n_o is the initial concentration of charge carriers in trap levels, ν is frequency factor, β is heating rate, T_0 is beginnig temperature of heating treatment and b is order of kinetics. The curve showing the temperature dependence of TL intensity obtained from measurements is called as TL glow curve. Activation energies of the trap levels, frequency factor and order of kinetics are obtained from the analyses of glow curve. There are many analyses methods to calculate these parameters. Some of these methods applied throughout this thesis are mentioned below.

2.5.3.3 Curve Fitting

Theoretical equations 2.4, 2.5 and 2.6 can be simplified under some assumptions such as independency of ν from temperature. When the integrals are solved by integration by parts, they can be simplified to simple polynomial functions (Yuksek et al., 2003). These functions are defined to suitable computer programmes and observed TL glow curve can be fitted. That means curve fitting method is based on fitting of the TL peak(s) using simplified equations by suitable software programme. The fitting parameters give us opportunity to obtain activation energy,

peak maximum temperature, frequency factor and order of kinetics. The software programme also helps to separate overlapped peaks when the TL intensities of more than one overlapped peak are defined to software as summation of individual peaks.

2.5.3.4 Initial Rise Method

Initial rise technique is an effective method used for decades to get the activation energies of trap level(s) (Chen & Kirsh 1981). Integrals defined for TL intensity for each of kinetics are very small in the initial ascending part of the TL curve. For that reason, the given integrals above is simplified in this initial part of the curve as

$$I = C\exp(-E_t / kT) \ , \tag{2.7}$$

where C is constant. If the graph of ln (I) versus 1/T is plotted, a straight line with a slope of ($-E_t / k$) is obtained. As stated, the most effective property of this method is the usability for all order of kinetics.

2.5.3.5 Peak Shape Method

Peak shape method uses the temperature values T_m, T_l and T_h where T_m is the peak maximum temperature, T_l and T_h are the low and high half-intensity temperatures, respectively (Chen & Kirsh 1981). In the peak shape analyses three parameters, $\tau = T_m - T_l$, $\delta = T_h - T_m$ and $w = T_h - T_l$ are used. Activation energy related with observed peak is found from average of energies of

$$E_\tau = \left[1.51 + 3.0(\mu_g - 0.42)\right] kT_m^2 / \tau - \left[1.58 + 4.2(\mu_g - 0.42)\right] 2kT_m \tag{2.8}$$

$$E_\delta = \left[0.976 + 7.3(\mu_g - 0.42)\right] kT_m^2 / \delta \tag{2.9}$$

$$E_w = \left[2.52 + 10.2(\mu_g - 0.42)\right] kT_m^2 / w - 2kT_m \ , \tag{2.10}$$

where $\mu_g = \delta/w$. The μ_g parameter is considered as 0.42 and 0.52 for first and second-order kinetics, respectively (Chen & Kirsh 1981).

CHAPTER 3

EXPERIMENTAL DETAILS

Shallow trapping levels in MgO were searched by photo-transferred TL experiments in 10-300 K temperature range. In addition to thermoluminescence measurements, structural properties of the used nanoparticles were studied by means of x-ray diffraction (XRD), scanning electron microscopy (SEM) and Fourier-transform infrared (FTIR) spectroscopy. In the present chapter, details of the experimental techniques and used devices are given.

3.1 X-ray Diffraction

XRD method was accomplished to seek the crystal structure of MgO nanoparticles. Figure 3.1 indicates used device of "Rigaku miniflex" diffractometer for this purpose. It works with CuKα radiation ($\lambda = 0.154049$ nm). The experiments were done using powders of MgO nanoparticles in the diffraction angle range of 10-90^{o}. The x-ray diffraction data was analyzed by the help of "TREOR 90" software program.

3.2 Scanning Electron Microscopy

The surface morphology of MgO nanoparticles was recorded by scanning electron microscope (Nova NanoSEM 430, FEI LTD). Figure 3.2 presents the used microscope for this purpose.

Figure 3.1 Rigaku miniflex diffractometer.

Figure 3.2 Used scanning electron microscope

3.3 Fourier Transform Infrared Spectroscopy

Transmittance spectrum of MgO nanoparticles was obtained in the infrared region using Nicolet 6700 FTIR spectrometer (Thermo Scientific, USA) indicated in Fig. 3.3. Spectrometer has He/Ne laser source (632.8 nm), KBr beamsplitter, DTGS-Kbr detector. The spectral range used in experiments was 400 and 4000 cm^{-1}. A software program named as OMNIC was used to scan the nanoparticles and record output data.

Figure 3.3 Nicolet 6700 FTIR spectrometer

3.4 Thermoluminescence Measurements

MgO nanopowders were provided from Alfa Aesar. The pellet disk forms of the MgO nanoparticles with diameter of 10 mm and thickness of ~1 mm were used in TL experiments. Pellets were subjected to Sr^{90}/Y^{90} beta radiation at 300 K. This beta irradiation helps to fill all shallow and deep trapping centers at room temperature. However, charge carriers in the shallow trap centers have big probability to escape

from these centers. Therefore, shallow centers are empty at room temperature. The beta radiated pellets were placed inside a closed cycle helium gas cryostat (Advanced Research Systems, Model CSW-202). LakeShore Model 331 temperature controller was used to heat the sample linearly by 1.0 K/s. Figure 3.4 shows a simple diagram of the used system for thermoluminescence experiments.

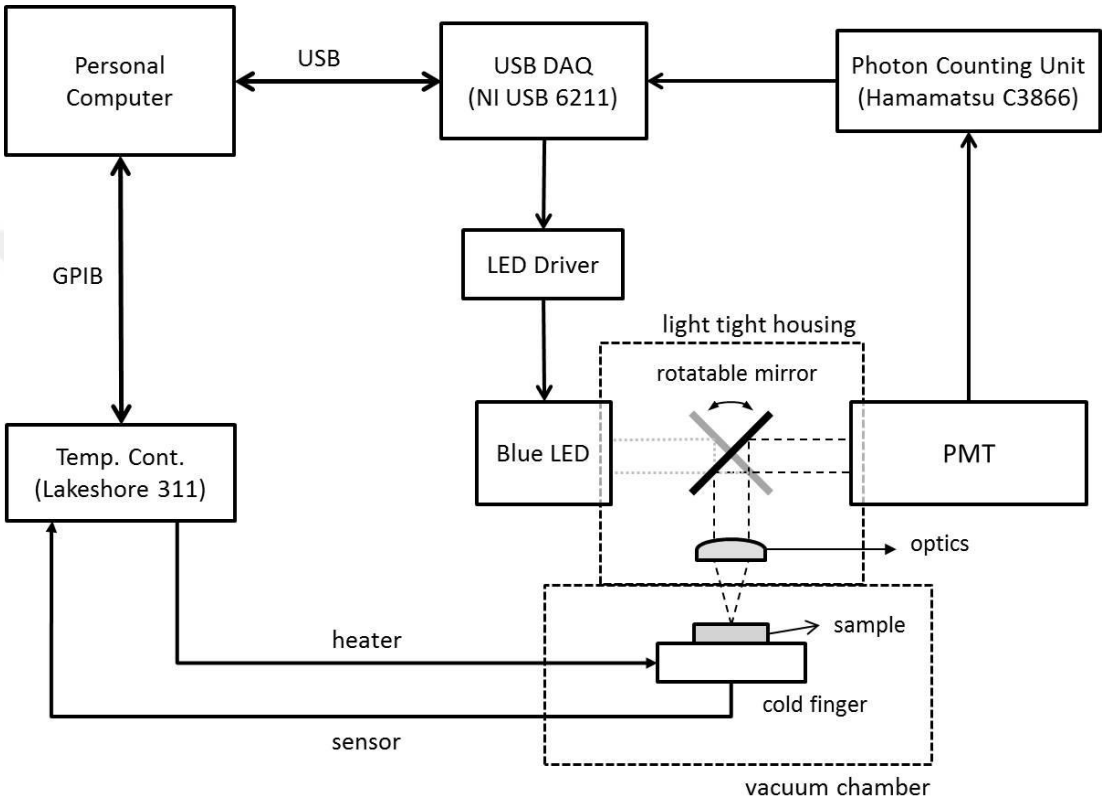

Figure 3.4 Simple diagram of low temperature thermoluminescence set-up [Isik et al., 2013].

The transfer of charge carriers from deep levels to shallow levels was achieved at 10 K by illuminating the pellets using blue LED (~2.6 eV). Charge carriers in deep centers were excited firstly to delocalized bands and then trapped at shallow levels. MgO nanopowders were illuminated for 120 seconds at low temperature T_0 = 10 K, after 120 seconds of waiting in dark, the temperature of the system was increased linearly.

CHAPTER 4

RESULTS AND DISCUSSION

MgO nanoparticles were characterized using XRD, SEM, FTIR and phototransferred TL techniques. In the present chapter, the results of each used experimental method were given in detail. Moreover, obtained results and values were compared and/or associated with those of previously reported papers on MgO samples.

4.1 Results of X-ray diffraction measurements

Figure 4.1 shows XRD pattern of MgO nanoparticles in the range of 10-90º. Lattice parameters of nanoparticles were obtained by software called as "TREOR 90". The analyses resulted in cubic structure with a = 0.4186 nm. Furthermore, Miller indices of diffraction peaks presented in figure were found using software. The revealed lattice parameter and Miller indices are in good agreements with those reported in JCPDS card with No:01-1235. Table 4.1 reports Miller indices, 2θ values, observed interplanar spacings (d) and relative intensities of the observed peaks.

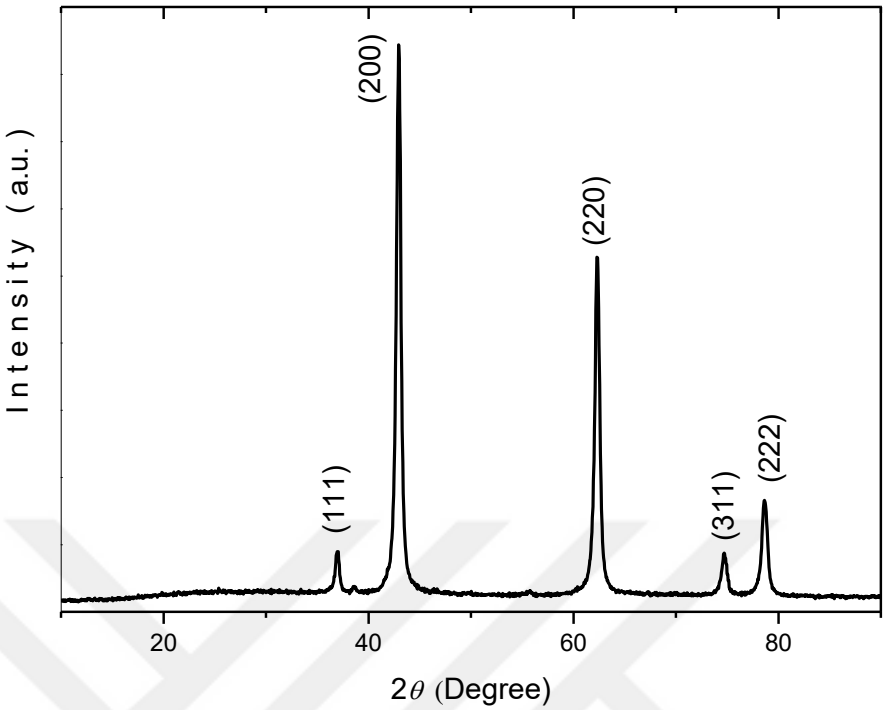

Figure 4.1 X-ray diffractogram of MgO nanoparticles.

Table 4.1. X-ray powder diffraction data for MgO nanoparticles

2θ	*h k l*	d_{obs} (nm)	I / I_0
37.00	1 1 1	0.24276	7.3
42.95	2 0 0	0.21041	100
62.30	2 2 0	0.14891	61.0
74.70	3 1 1	0.12697	5.7
78.65	2 2 2	0.12155	16.6

The diffraction peaks presented in XRD figure can be used to get knowledge about nanoparticle size. The peaks are analyzed by Debye-Scherrer's expression given as (Cullity & Stock 2001)

$$D = \frac{0.9\lambda}{\beta cos\theta} \quad . \tag{4.1}$$

In the equation 4.1, D, β and $\cos\theta$ correspond to crystalline size, full-width at half maximum and diffraction angle, respectively. This equations refers that slope of $\cos\theta$ vs. $1/\beta$ is equal to $0.9\lambda/D$. Figure 4.2 indicates the relevant data and its linear fit. The average nanoparticle size was found as 29 nm under the light of equation 4.1.

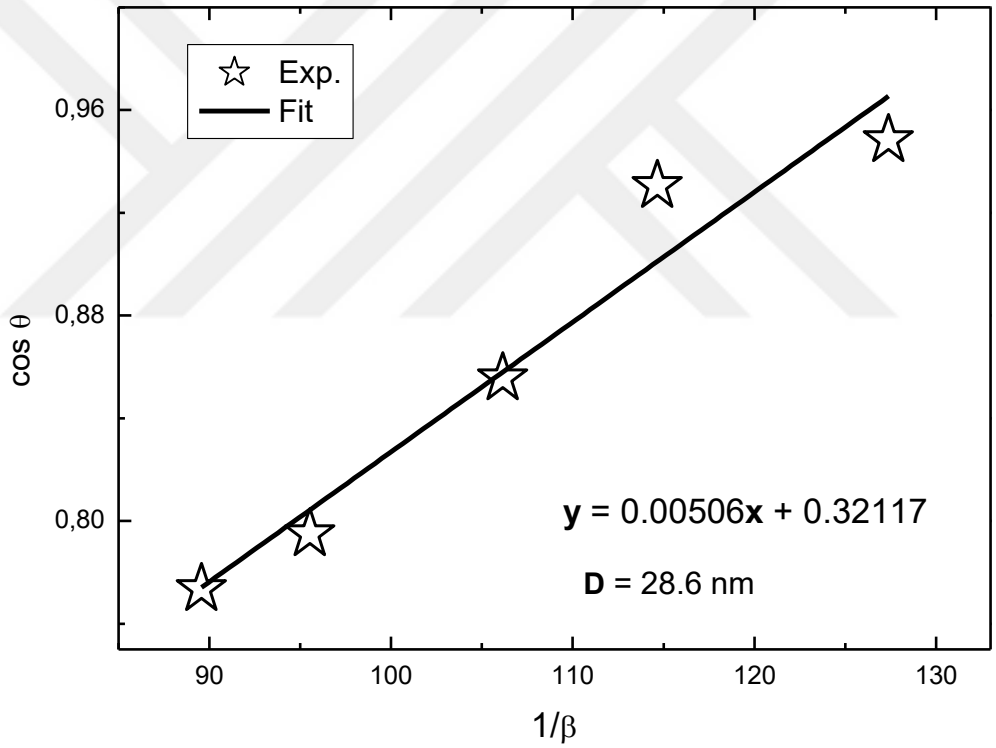

Figure 4.2. Debye-Scherrer analyses according to Eq. 4.1

XRD peaks can be utilized to get knowledge about strain occuring due to crystal imperfections. Williamson and Hall analyses gives probability to obtain strain and crystalline size. Uniform deformation model is expressed as (Birkholz 2006)

$$\beta\cos\theta = \frac{k\lambda}{D} + 4\varepsilon\sin\theta \quad . \tag{4.2}$$

According to this model, strain is assumed as uniform in all directions of crystalline. According to this equation, $\beta\cos\theta$ vs. $4\sin\theta$ plot results in a slope of ε (strain) and y-intercept of fitted line which is equal to $k\lambda/D$. Figure 4.3 shows the relevant plot and its linear fit. The strain and crystalline size were obtained as 6.9×10^{-4} and 19.5 nm, respectively.

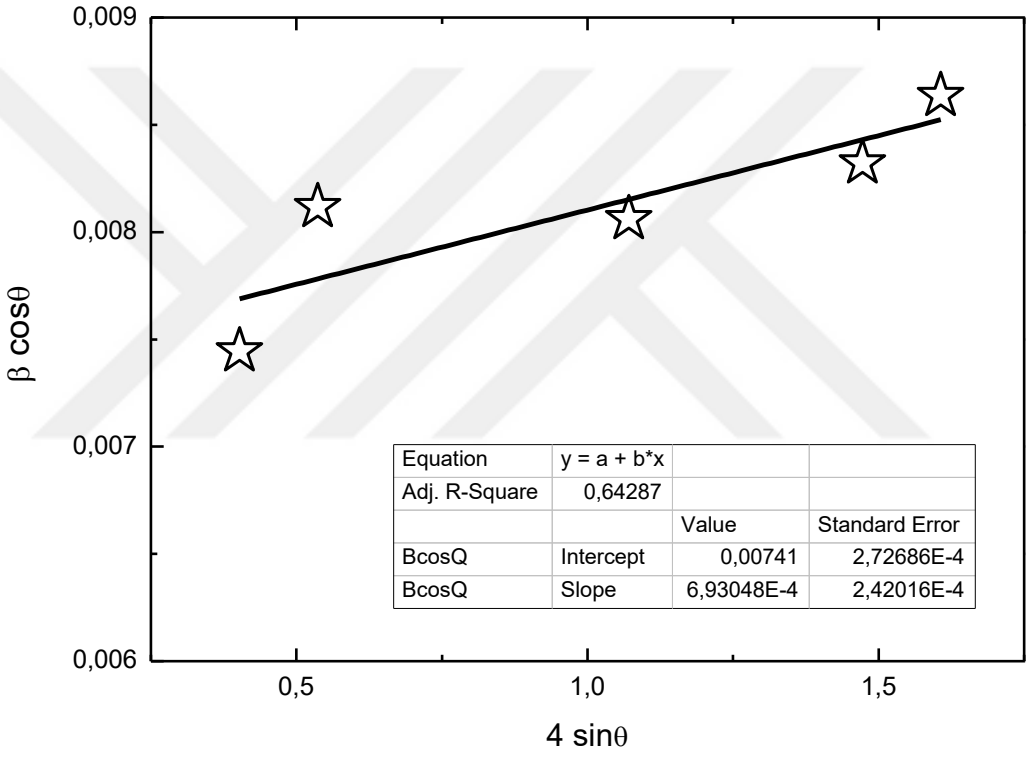

Figure 4.3 Williamson-Hall analyses of MgO nanopowders

4.2 Results of Scanning Electron Microscopy Measurements

SEM method was performed to obtain knowledge about the surface morphology of nanoparticles. Figure 4.4 indicates the SEM images of MgO nanoparticles used as powder form in measurements for two different resolutions.

Used samples are observed in the form of nanoparticles with particle size generally around ~30-50 nm.

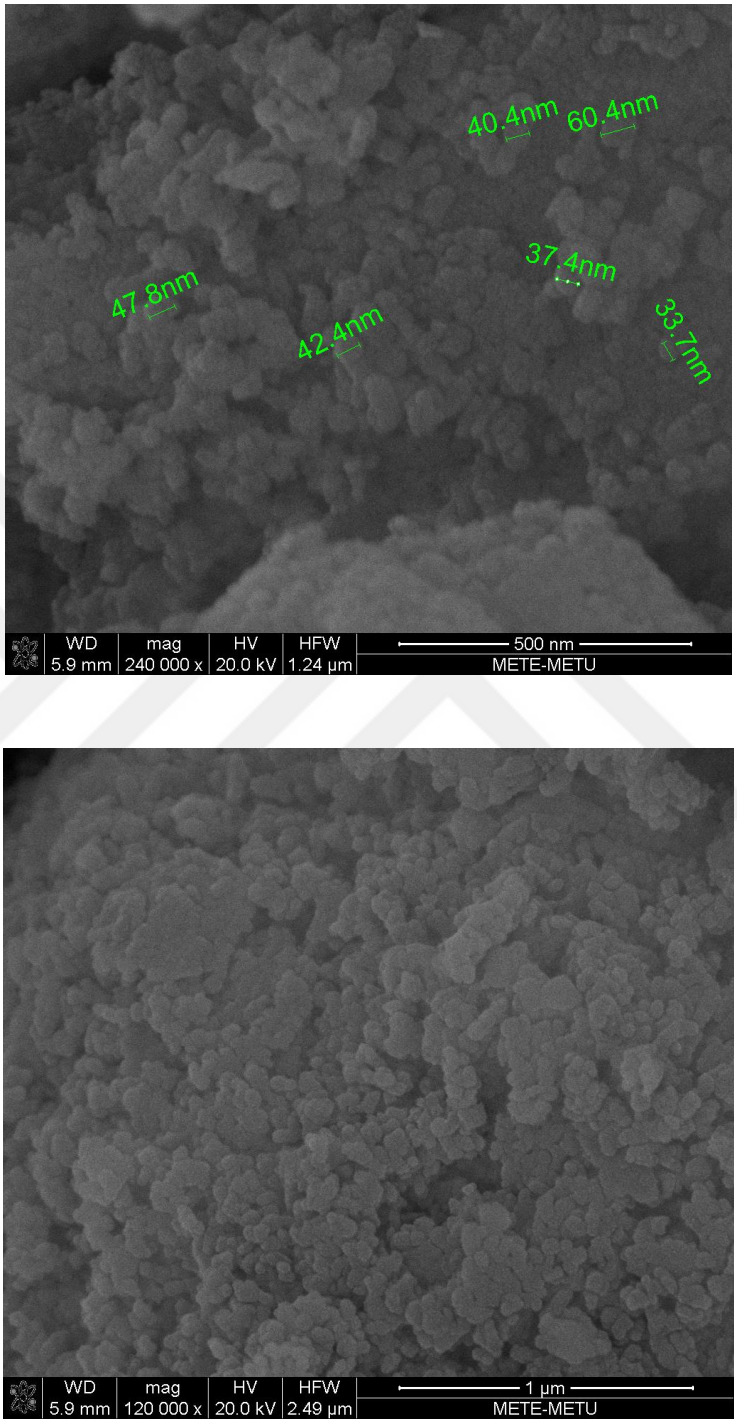

Figure 4.4 SEM images of MgO nanoparticles.

4.3 Results of FTIR Measurements

Infrared transmittace spectrum of MgO nanopowders was obtained by FTIR measurements in the region of 400-4000 cm^{-1}. The spectrum and observed bands are shown in Fig. 4.5. Spectrum indicates minima positions around 653, 668, 680, 720, 935, 2270, 2342 and 2358 cm^{-1}. According to previously reported studies, 668 cm^{-1} was attributed to different Mg-O-Mg vibration modes. The minima positions observed between 400-900 cm^{-1} were thought because of Mg-O vibrational mode [Sutradhar et al., 2011].

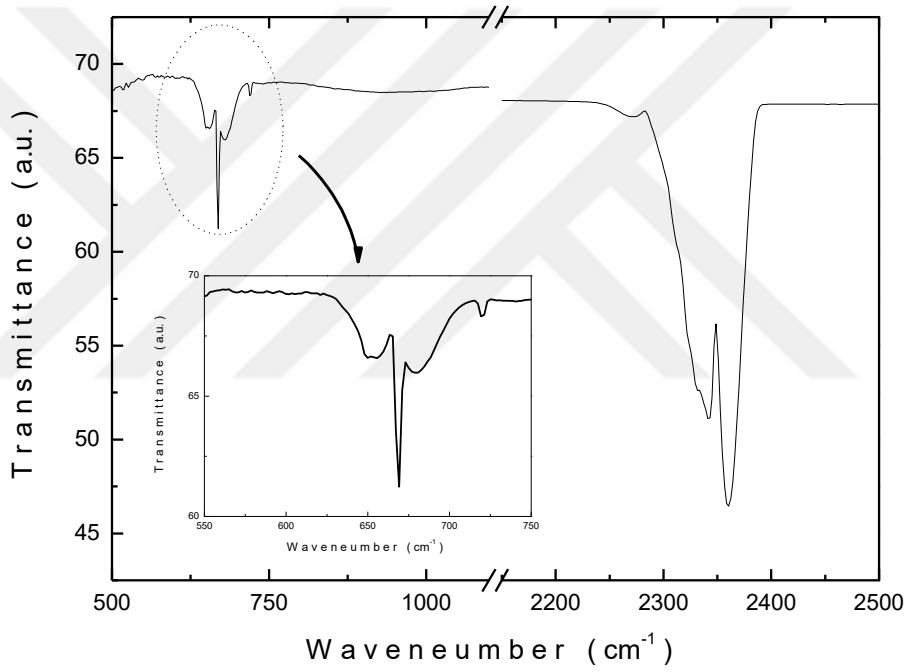

Figure 4.5 Infrared transmittance spectrum of MgO nanopowders

4.4 Results of Thermoluminescence Measurements

Shallow trapping centers in MgO nanopowders were searched using photo-transferred thermoluminescence (PTTL) experiments. TL and PTTL differ according to the filling process/source of shallow trapping centers. In the TL process (see Fig.

4.6), material is illuminated at low temperature by excitation source having energy greater than band gap (E_g = 7.8 eV). When charge carriers excited to conduction band (process (1)) are captured by shallow and deep trapping centers (process (2)). At low temperature, these trapped charges do not have sufficient energy to be excited to conduction band from trap centers. When the illumination is turned off and then sample is heated, charges having enough energy (by means of heat) to be excited to conduction band (process (3)). These excited electrons recombine with holes (process (4)) and give emission to outside.

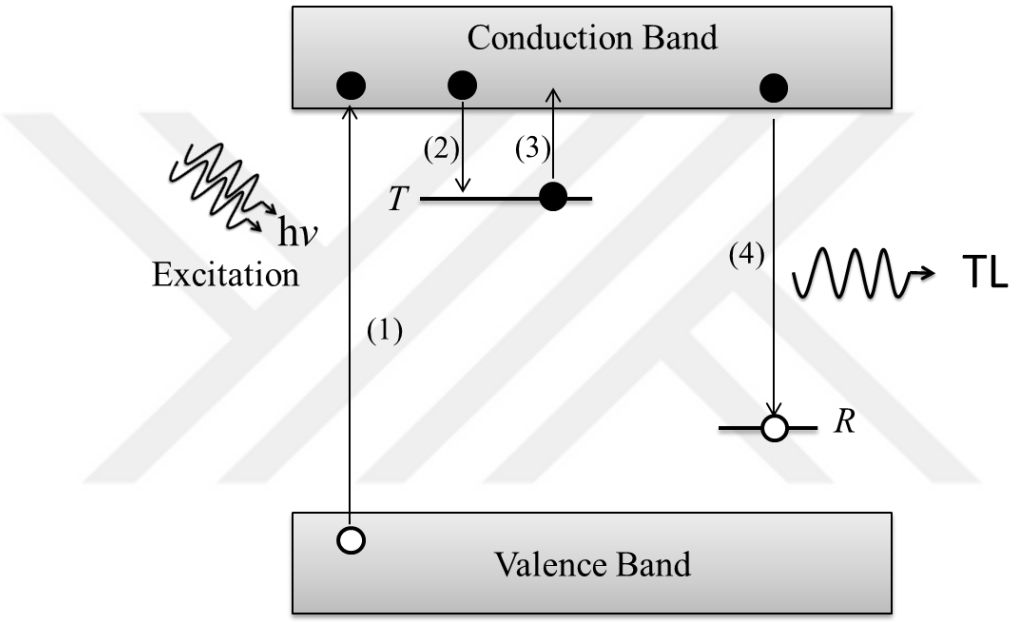

Figure 4.6 Simple diagram showing physical processes in TL experiments.

In our experiments, we used photo-transferred thermoluminescence technique. The simple figure showing all processes in PTTL experiments is indicated in Fig. 4.7. The excitation of material is done at 300 K by β-radiation. We excited the sample at room temperature due to technical problems. Charges excited from valence to conduction band (process (1)) are captured by shallow and deep centers (process (2)). However, electrons in shallow trapping levels have sufficient energy at 300 K to escape from these levels. Trapped charges in deep levels do not have enough energy. For that reason, they occupy their levels at room temperature. After cooling the sample/system to 10 K, sample was subjected to blue light having energy ~2.6 eV.

Since this energy is smaller than band gap, additional charges cannot be excited to conduction band. However, charges from trap levels at energy positions smaller than 2.6 eV can excite to conduction band and then captured at shallow centers (process (3)). Since, the charges in these shallow centers do not have sufficient energy to escape from their centers at T = 10 K, they take role in TL measurements. When the sample temperature is increased, these charges follow the paths shown by process (4).

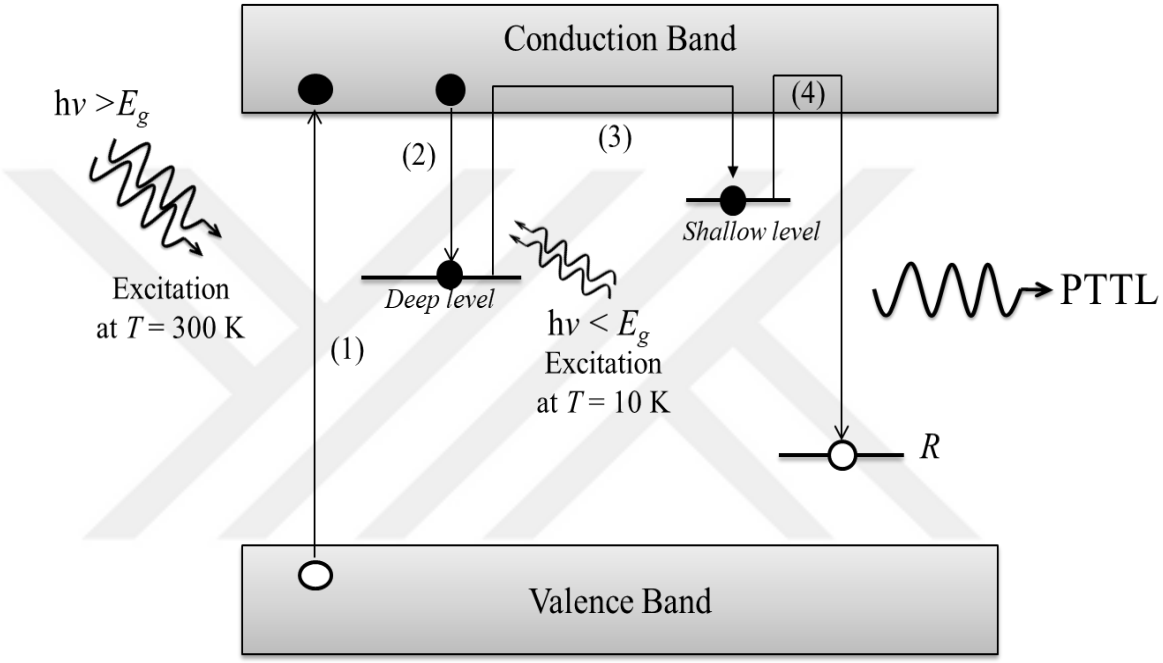

Figure 4.7 Simple diagram showing physical processes in PTTL experiments.

Figure 4.8 indicates the PTTL glow curve recorded at rate of 1 K/s. PTTL spectrum presents one peak around 150 K. Analyses of this peak were carried out by curve fitting, initial rise and peak shape techniques.

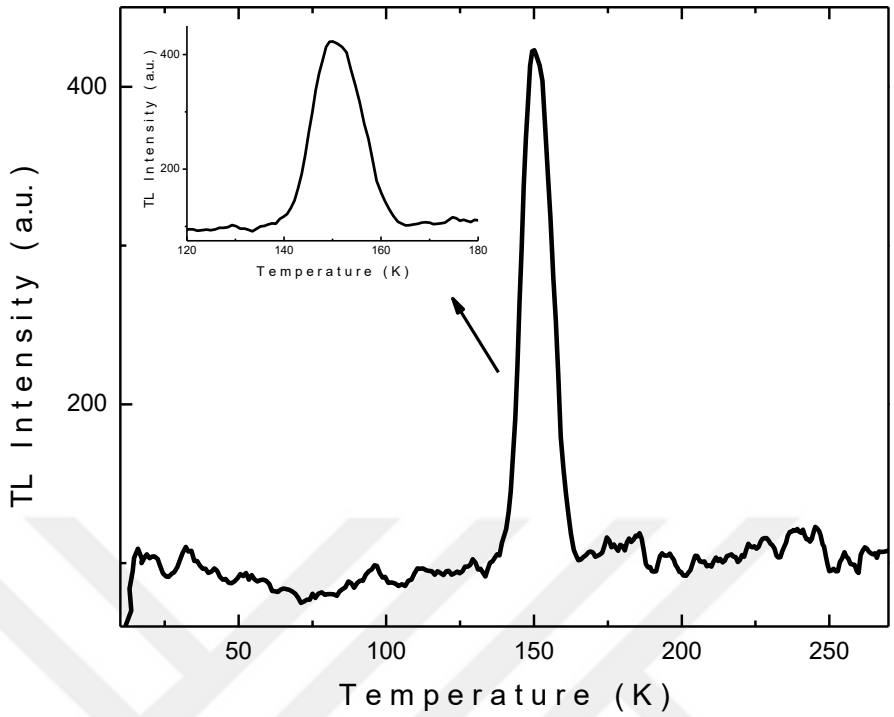

Figure 4.8 PTTL glow curve of MgO nanopowders.

Curve fit technique is based on fitting of experimental data using theoretical equations. PTTL curve presented in Fig. 4.8 shows one peak. Therefore, we tried to fit this peak by assuming one trap level associated with this peak. Fig. 4.9 shows the experimental curve (stars) and fitted curves for slow retrapping (blue curve) and fast retrapping (red curve) cases. It is seen that fitting treatment under the light of slow retapping is not successful. The fitting applied considering the second order of kinetics seems a little bit acceptable. When the starting and ending regions of the curve were considered, fitted curve and experimental curve do not successfully overlapped.

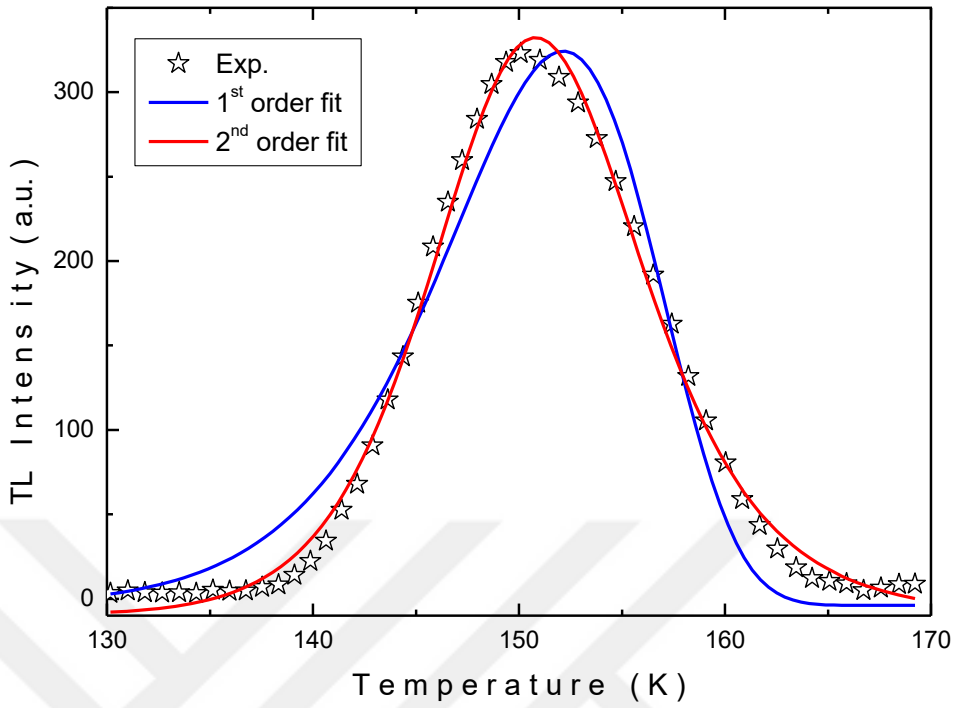

Figure 4.9 Experimental curve (stars) and fitted curves for slow retrapping (blue curve) and fast retrapping (red curve) cases

Parameter of μ_g expressed in peak shape technique is given as $\mu_g = \frac{T_h - T_m}{T_h - T_l}$ where T_h, T_l and T_m symbolize the low and high half-intensity temperatures, peak maximum temperature, respectively. The μ_g is considered as 0.42 and 0.52 for first and second-order kinetics, respectively (Chen & Kirsh 1981). This parameter get values between 0.42 and 0.52 for general order of kinetics. This parameter was found as 0.58 for observed peak. This value is not between 0.42 and 0.52. These points; i) unsuccessful fitted curve, ii) inappropriate μ_g value; indicate that observed peak is composed of more than one single peak.

Figure 4.10 shows the fitting result by considering that observed peak (stars) is composed of two discrete peaks (dash-dotted curves) associated with two various trap levels in MgO nanopowder. Curve fit application resulted with activation energies of E_{tA} = 0.70 eV and E_{tB} = 0.91 eV (Table 4.2). Furthermore, fitting process was successfully achieved for the case of second order of kinetics.

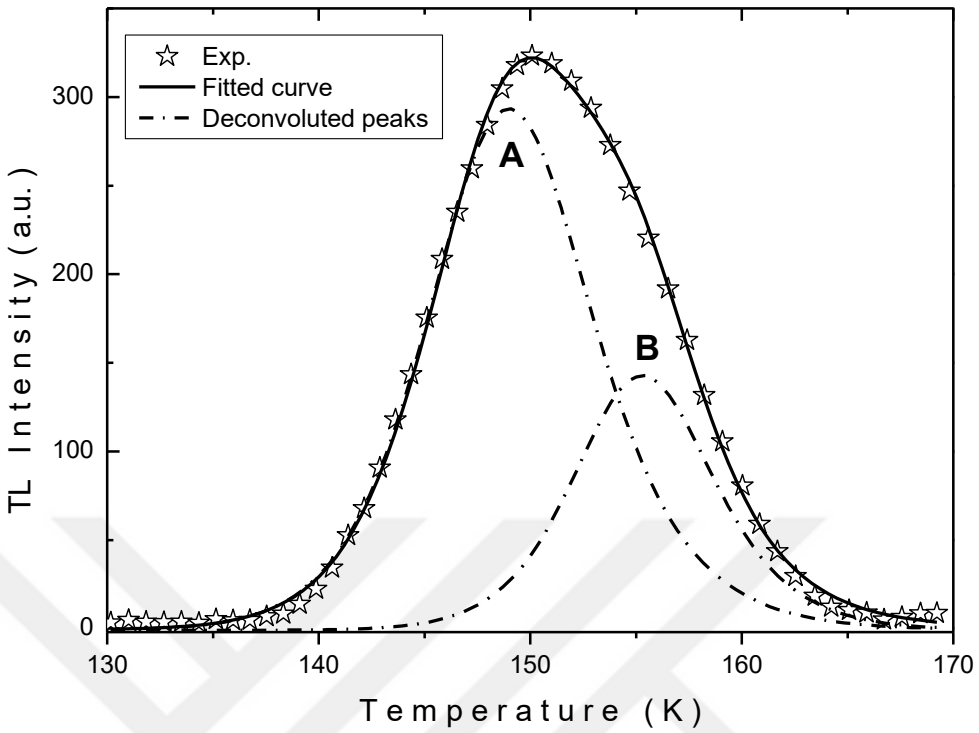

Figure 4.10. Experimental TL curve (stars) and fitted curve (solid line). Dash-dotted curves represent the deconvoluted peaks

Table 4.2. The activation energy (E_t), peak maximum temperature (T_m) and parameter μ_g of traps for two TL peaks of MgO nanopowder.

Peak	T_m(K)	E_t (eV)			μ_g
		Curve fitting method	Initial rise method	Peak shape method	
A	149.0	0.70	0.69	0.67	0.50
B	155.3	0.91	0.92	0.88	0.51

PTTL peak was also analyzed by initial rise (IR) and peak shape (PS) techniques. IR method is based on the theoretical fact of that PTTL intensity is proportional to $\exp(-E_t/kT)$ at the instant peak starts to appear (Chen & Kirsh 1981). This points out that slope of ln(I_{TL}) vs. 1/T gives $(-E_t/kT)$. Figure 4.11 shows associated plots. Ativation energy values of trapping levels were obtained as E_{tA} = 0.69 eV and E_{tB} = 0.92 eV (Table 4.2).

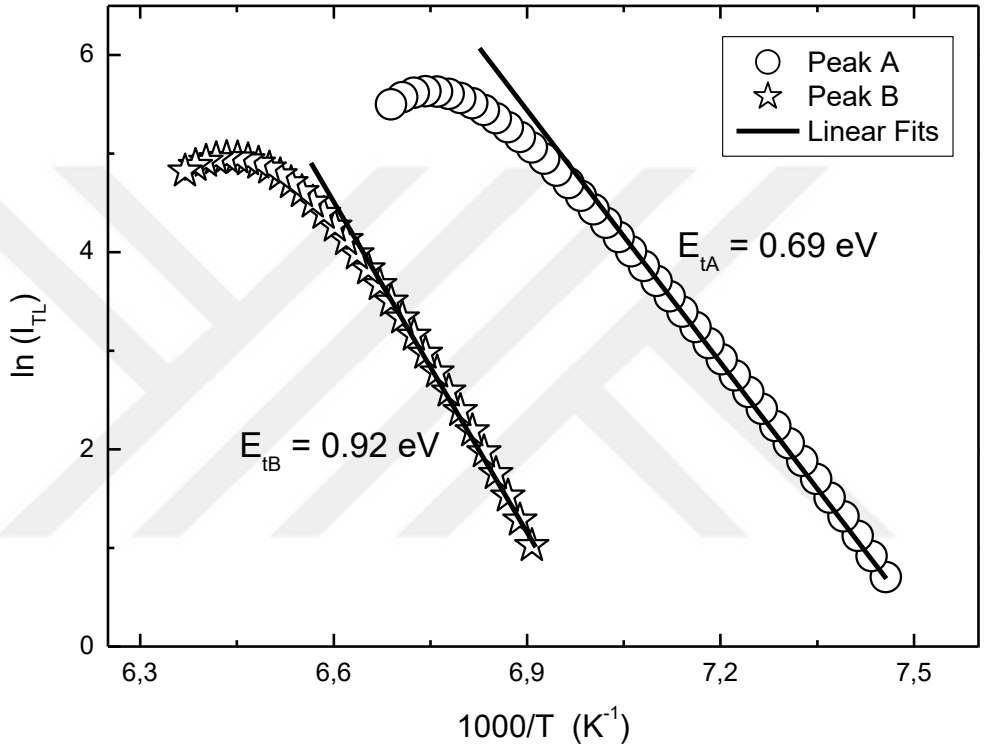

Figure 4.11 The plots for initial rise method analyses.

Activation energies of trap levels were also calculated using peak shape method. The average values of activation energies E_ζ, E_δ and E_w defined in chapter 2 were calculated as E_{tA} = 0.67 eV and E_{tB} = 0.88 eV (Table 4.2). The μ_g parameter for these peaks were calculated and found closer to 0.52 which indicates the presence of dominant mechanism of fast retrapping. All obtained activation energy values of peaks by curve fitting, initial rise and peak shape methods are in good agreement with each other.

An energy diagram presented in Fig. 4.12 was plotted by taking into account the obtained energy values. This diagram shows transitions in PTTL experiments. MgO nanopowders were subjected to Sr^{90}/Y^{90} beta source at room temperature. Excited charges to conduction band were trapped in deep centers. At T = 300 K, shallow centers are not stable. Shallow trapping levels were filled T = 10 K by irradiating the nanoparticles by blue LED. The excited charges from shallow levels were recombined and emitted luminescence.

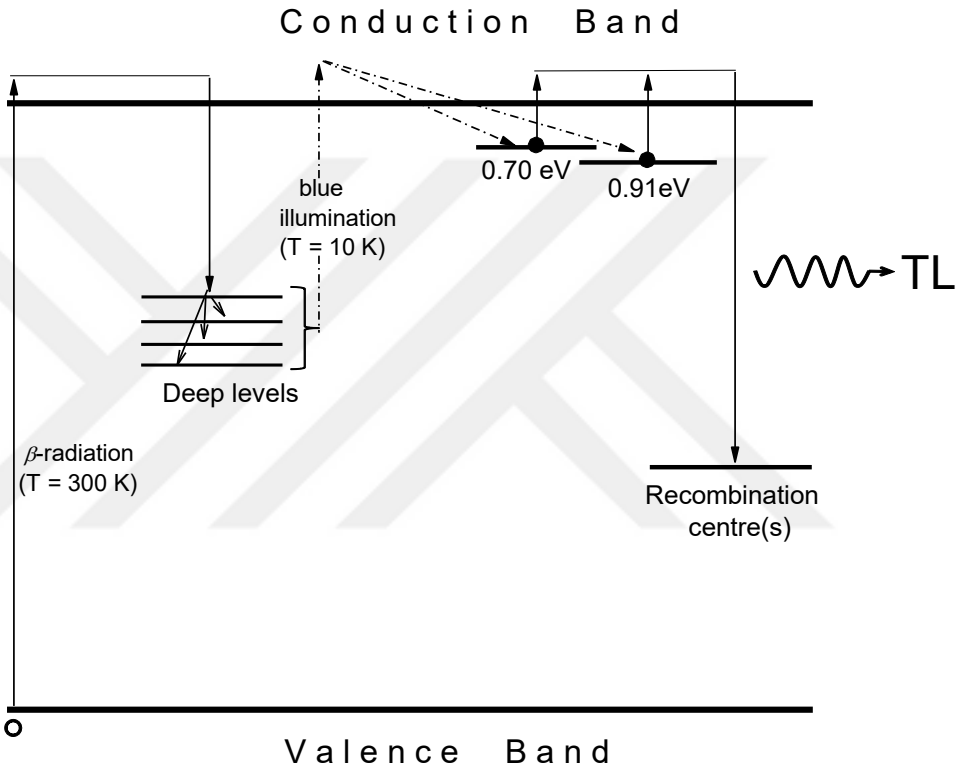

Figure 4.12 Simple energy level diagram of MgO presenting transitions in PTTL.

CHAPTER 5

CONCLUSION

Structural and TL properties of MgO nanopowders were reported in the present thesis. Structural properties of studied samples were revealed using XRD, SEM and FTIR experimental methods. X-ray diffraction pattern indicated five sharp peaks which are well correlated with cubic structure of lattice parameter 0.4186 nm. X-ray diffraction peaks were also used to determine the particle size and lattice strain of the sample. Debye-Scherrer analyses showed that average size of nanoparticles is equal to 29 nm. Lattice strain and crystalline size were obtained using Williamson-Hall method. The analyses resulted in lattice strain of 6.9×10^{-4} and crystalline size of 19.5 nm. Scanning electron microscope images were used to get knowledge about the surface morphology of the samples. The particle size of nanoparticles were measured between ~30-50 nm from the images. Infrared transmittance spectrum of the used samples was also revealed using FTIR technique. In the spectrum, some minima positions related with phonon absorption were observed. When observed bands in the range of 400-900 cm^{-1} were compared with previously reported values, it was noticed that these bands are due to Mg-O different vibrational modes.

Shallow trap levels in MgO nanopowders were searched by PTTL experiments in the temperature region of 10-300 K. Shallow trapping levels were filled by charge carriers excited from deep centers. The glow curve presented one peak around 150 K. Unsuccessful curve fitting result and peak shape method parameter μ_g of the observed peak indicated that this one peak is not composed of one single peak. Therefore, analyses were done under the light of the thought of presence of two single peaks. All applied methods; curve fitting, initial rise and peak shape methods, showed that activation energies of the trap levels associated with deconvoluted two

single peak is 0.70 and 0.91 eV. Curve fit application was succesfully resulted for the fitting process corresponding to second order kinetics stating that fast retrapping is dominant transition mechanism in the PTTL process.

REFERENCES

Birkholz, M. (2006). *Thin Film Analysis by X-ray Scattering.* Wiley-VCH Verlag GmbH and Co. KGaA, Weinheim.

Bragg, W.L. (1913). The reflection of x-rays by crystals. *Proceedings of the Royal Society of London Series* A. 17, 43-53

Chen R., Kirsh, Y. (1981). *Analysis of Thermally Stimulated Processes,* Pergamon Press, Oxford.

Choudary, B.M., Mulukutla, R.S., Klabunde, K.J. (2003). Benzylation of aromatic compounds with different crystallites of MgO. *J. Am. Chem. Soc*. 125, 2020-2021.

Cullity, B.D., Stock, S.R. (2001). *Elements of X-ray Diffraction*, Prentice Hall, New Jersey.

Devaraja, P.B. Avadhani, D.N., Prashantha, S.C., Nagabhushana, H., Sharma, S.C., Nagabhushana, B.M., Nagaswarupa, H.P., Premkumar, H.B. (2014). MgO:Eu_{3+} red nanophosphor: low temperature synthesis and photoluminescence properties. *Spectrochim. Acta A Mol. Biomol. Spectrosc.* 121, 46–52.

Dong, W.J. Li, B.J., Li, Y., Wang, X.B., An, L.N., Li, C.R. (2011). General approach to well defined perovskite $MTiO_3$ (M = Ba, Sr, Ca, and Mg) nanostructures. *J. Phys. Chem. C* 115, 3918–3925.

Fletcher, P.R., Leach, C. (1995). Quality assessment of MgO substrate materials for high T-C superconductor thin films using cathodoluminescence microscopy. *J. European Ceramic Soc.* 15, 859-865.

Huang, L., Li, D.Q., Lin, Y.J., Wei, M., Evans, D.G., Duan, X. (2005). Controllable preparation of nano-MgO and investigation of its bactericidal properties. *J. Inorg. Biochem.* 99, 986-993.

Isik, M., Bulur, E., Gasanly, N.M. (2013). Low temperature thermoluminescence in $TlGaS_2$ layered single crystals. *J. Lumin.* 135, 60-65.

Jalili, S., Majidi, R. (2008). The effects of impurities on the electronic properties of MgO. *Physica B.* 403, 3522-3526.

Kadri, D., Mokeddem, A., Hamzaoui, S. (2005). Intrinsic defects in UV-irradiated MgO single crystal detected by Thermoluminescence. *J. Appl. Sci.* 5, 1345-1349.

Kato, T., Okada, G., Yanagida, T. (2016a). Optical, scintillation and dosimeter properties of MgO transparent ceramic doped with Mn^{2+}. *J. Ceram. Soc. Jpn.* 124, 559-563.

Kato, T., Okada, G., Yanagida, T. (2016b). Optical, scintillation and dosimeter properties of MgO translucent ceramic doped with Cr^{3+}. *Optical Materials.* 54, 134-138.

Kittel, C. (1971). *Introduction to Solid State Physics*, Wiley, New York.

Kronig, R.L., Penney, W.G. (1930). Quantum Mechanics of Electrons in Crystal Lattices. *Proc. Roy. Soc. (London).* 130, 499-513.

McKeever, S.W.S. (1985). *Thermoluminescence of solids*, Cambridge Uni. Press, Cambridge.

Oliveira, L.C., Doull, B.A., Yukihara, E.G. (2013b). Investigations of MgO:Li,Gd thermally and optically stimulated luminescence. *J. Lumin.* 133, 282-289.

Oliveira, L.C., Milliken, E.D., Yukihara, E.G. (2013a). Development and characterization of MgO:Nd,Li synthesized by solution combustion synthesis for 2D optically stimulated luminescence dosimetry. *J. Lumin.* 133, 211-216.

Oliveira, L.C., Yukihara, E.G., Baffa, O. (2016). MgO:Li,Ce,Sm as a high-sensitivity material for Optically Stimulated Luminescence dosimetry. *Sci. Rep-UK.* 6, 24348.

Park, J.Y., Lee, Y.J., Jun, K.W., Baeg, J.O., Yim, D.J. (2006). Chemical synthesis and characterization of highly oil dispersed MgO nanoparticles. *J. Ind. Eng. Chem.* 12, 882–887.

Sathyamoorthy, A., Luthra, J.M. (1978). Mechanism of thermoluminescence in magnesium oxide. *J. Mater. Sci.* 13, 2637-2644.

Selvam, N.C.S., Kumar, R.T., Kennedy, L.J., Vijaya, J.J., Comparative study of microwave and conventional methods for the preparation and optical properties of novel MgO micro and nanostructures. (2011). *J. Alloys Compd.* 509, 9809–9815.

Shang, L., Li, B.J., Dong, W.J., Chen, B.Y., Li, C.R., Tang, W.H. (2010). Hetero nanostructure of Ag particle on titanate nanowire membrane with enhanced photocatalytic properties and bactericidal activities. *J. Hazard. Mater*. 178, 1109–1114.

Shao, C., Guan, H., Liu, Y., Mu, R. (2006). MgO nanofibres via an electrospinning technique. *J. Mater. Sci.* 41, 3821–3824.

Stark, J.V., Klabunde, K.J. (1996). Nanoscale metal oxide particles/clusters as chemical reagents. Adsorption of hydrogen halides, nitric oxide, and sulfur trioxide on magnesium oxide nanocrystals and compared with microcrystals. *J. Chem. Mater.* 8, 1913-1918.

Sutradhar, N., Sinhamahapatra, A., Pahari, S.K., Pal, P., Bajaj, H.C., Mukhopadhyay, Panda, A.B. (2011). Controlled synthesis of different morphologies of MgO and their use as solid base catalysts. *J. Phys. Chem. C.* 115, 12308-12316.

Tamboli, S. H., Patil, R., Kamat, S., Puri, V., Puri, R. (2009). Modification of optical properties of MgO thin films by vapour chopping. *J. Alloys Compd.* 477**,** 855–859.

Tardio, M.M., Ramirez, R., Gonzalez, R., Chen. Y. (2002). p-type semiconducting properties in lithium-doped MgO single crystals. *Phys. Rev. B.* 66, 134202.

Xu, X.L., Asher, S.A. (2004) Synthesis and utilization of monodisperse hollow polymeric particles in photonic crystals. *J. Am. Chem. Soc.* 126, 7940–7945.

Yacobi, B.G. (2003). *Semiconductor Materials; An Introduction to Basic Principles*, Kluwer Academic, New York.

Yan, Y., Zhou, L., Zhang, J., Zeng, H., Zhang, Y., Zhang, L. (2008). Synthesis and growth discussion of one-dimensional MgO nanostructures: nanowires, nanobelts, and nanotubes in VLS mechanism. *J. Phys. Chem. C*. 112, 10412–10417.

Yuksek, N.S., Gasanly, N.M., Ozkan, H. (2003). Thermally stimulated current analysis of shallow levels in $TlGaS_2$ layered single crystals. *Semicond. Sci. Tech*. 18, 834-838.

Zhao, H.X., Dong, W.J., Zheng, Y.Y., Liu, A.P., Yao, J.M., Li, C.R. (2011). The structural and biological properties of hydroxyl apatite modified titanate nanowire scaffolds. *Biomaterials* 32, 5837–5846.

Zhao, W.R., Chen, H.R., Li, Y.S., Li, L., Lang, M.D., Shi, J.L. (2008). Uniform rattle type hollow magnetic mesoporous spheres as drug delivery carriers and their sustained-release property. *Adv. Funct. Mater*. 18, 2780–2788.